International Journal of Pharmaceutics: X 6 (2023) 100207

Contents lists available at ScienceDirect

International Journal of Pharmaceutics: X

journal homepage: www.sciencedirect.com/journal/international-journal-of-pharmaceutics-x

The shelf life of ASDs: 2. Predicting the shelf life at storage conditions

Friederike Wolbert [a,b], Christian Luebbert [c], Gabriele Sadowski [b,*]

[a] INVITE GmbH, Drug Delivery innovation Center (DDiC), 51368 Leverkusen, Germany
[b] TU Dortmund University, Department of Biochemical and Chemical Engineering, Laboratory of Thermodynamics, Emil-Figge-Str. 70, D-44227 Dortmund, Germany
[c] amofor GmbH, Otto-Hahn-Str. 15, 44227 Dortmund, Germany

ARTICLE INFO

Keywords:
Amorphous solid dispersion
Physical stability
Water sorption
PC-SAFT
Crystallization kinetics
Long term stability
Shelf life prediction

ABSTRACT

Amorphous solid dispersions (ASDs) are a widely used formulation technology for poorly water-soluble active pharmaceutical ingredients (API). Depending on the API-polymer combination and API load in the ASD, the amorphous API might be thermodynamically metastable and crystallize over time. The crystallization onset is one critical factor that can define the shelf life of the ASD. Thus, for ASD formulations, long-term stability against crystallization of the API is of particular interest. This work presents a method for predicting the long-term physical stability of ASDs (crystallization onset time). The new approach combines the Johnson-Mehl-Avrami-Kolmogorov (JMAK) equation with classical nucleation theory. The shelf life predicted using the new approach depends on supersaturation (determined with PC-SAFT), viscosity (determined with WLF equation or Arrhenius equation) and two specific model parameters k' and B. The latter were fitted to a few fast crystallization-kinetics measurements above the glass transition of the ASD. An additional crystallization-kinetics measurement below the glass-transition temperature of the ASD was used to determine the Arrhenius parameters. Once all parameters are determined for a given API/polymer combination and manufacturing method, they are valid for any API load, temperature, and RH. The proposed approach allows predicting the shelf life (crystallization onset) of a potential ASD in early stage of development within a few days. It was successfully verified for ASDs stored at 25 °C and 10% RH or 60% RH.

1. Introduction

Formulation of an amorphous solid dispersion (ASD) is a promising method for stabilizing the amorphous state of an API. In ASDs, the API is dissolved in a highly viscous amorphous polymer matrix. However, in many cases, the API is supersaturated in the polymer and thus might crystallize over time (Newman, 2015). The period during which a metastable ASD does not crystallize is its maximum shelf life and is crucial for regulatory approval procedures. This shelf life is significantly shortened at high storage temperatures and high humidity. The crystallization rate depends on nucleation and crystal growth, which are primarily determined by the molecular mobility and supersaturation of the API in the ASD (Tung et al., 2009; Jackson, 1969). Accordingly, studying the crystallization kinetics with respect to the influences of molecular mobility and API supersaturation in the ASD is subject of current research (Liu et al., 2021; Ojo and Lee, 2021; Greco et al., 2012; Marsac et al., 2008; Mistry and Suryanarayanan, 2016; Yang et al., 2010; Luebbert et al., 2018; Luebbert and Sadowski, 2017; Wolbert et al., 2022a).

Liu et al (Liu et al., 2021). presented a study on the risk assessment of API crystallization in packaged ASD drug products. Their modeling of the physical stability of those ASDs considered crystal growth kinetics, the predicted moisture uptake by the packaged ASD during storage, and the impact of water sorption on the glass-transition temperature of the ASD. Based on this, they devised a mitigation strategy and a workflow as a decision tree to identify promising ASDs (Liu et al., 2021).

Ojo and Lee (Ojo and Lee, 2021) developed a mechanistic model to predict the physical stability of ASDs. Their approach incorporates kinetic and thermodynamic factors such as supersaturation of the API in the polymer, diffusivity, and interfacial energy of the ASD to model crystallization kinetics in ASDs. They also performed viscosity measurements over a wide temperature range to support the stability predictions. However, they only investigated the crystallization kinetics in their ASDs in the absence of humidity. As a result, they developed a

Abbreviations: API, Active Pharmaceutical Ingredient; ASD, Amorphous Solid Dispersion; DVS, Dynamic Vapor Sorption; GRI, Griseofulvin; JMAK, Johnson-Mehl-Avrami-Kolmogorov; PC-SAFT, Perturbed-Chain Statistical Associating Fluid Theory; PVPVA, Poly (vinylpyrrolidone-*co*-vinyl acetate); RH, Relative Humidity.

* Corresponding author.
E-mail address: gabriele.sadowski@tu-dortmund.de (G. Sadowski).

https://doi.org/10.1016/j.ijpx.2023.100207
Received 2 May 2023; Received in revised form 5 August 2023; Accepted 23 August 2023
Available online 25 August 2023

mechanistic model of five coupled ordinary differential equations. Their model predicts the shelf life of ASDs in good agreement with the experimental data (Ojo and Lee, 2021).

Greco et al (Greco et al., 2012). investigated the influence of temperature and moisture on the crystallization kinetics of ASDs. Their study suggested that the crystallization kinetics of HPMCAS ASDs only depend on the parameter T_g/T (with T_g being the glass-transition temperature and T being the storage temperature) but do not depend on RH, when below the glass-transition temperature. They could also show that the crystallization kinetics of ASDs for which the onset of crystallization is below three months can be extrapolated to a period of up to 15 months. Their methodology can be used as a stress program to predict shelf life from a relatively short observation period and to design appropriate conditions of temperature and humidity for long-term storage to prevent API crystallization. However, this method is only applicable if neither moisture nor supersaturation have a significant influence on the crystallization kinetics. This means that the crystallization-kinetics measurement performed at high temperatures and used for the estimation of the shelf life of ASDs at lower temperatures must be performed in the desired drug load. Thus, their approach cannot be used to extrapolate the crystallization kinetics to other drug loads or humidities (Greco et al., 2012).

The aim of this work is to predict the shelf life (crystallization onset) of ASDs at different storage conditions. For this purpose, the relationship between the shelf life of ASDs (i.e., their crystallization kinetics) and the most important factors affecting crystallization kinetics, such as type of polymer, storage temperature, relative humidity (RH), and API load was investigated. Subsequently, a modeling approach derived from classical nucleation theory (Mullin, 2001; Kalikmanov, 2013) and linked to the Johnson-Mehl-Avrami-Kolmogorov (JMAK) model was developed to predict the shelf life of ASDs. This approach requires the supersaturation of the API in the ASD, the viscosity of the ASD, and one crystallization-kinetics measurement above the glass-transition temperature. After presenting all building blocks for the shelf-life prediction, the developed modeling approach is applied to predict the shelf life of GRI/PVPVA and GRI/Soluplus ASDs stored at 25 °C/10% RH and 25 °C/60% RH. The predicted shelf lifes are compared with measured shelf lifes.

The proposed modeling approach is rather simple (compared to the complex classical nucleation theory (Mullin, 2001; Kalikmanov, 2013)) and can be successfully used to extrapolate/predict the shelf life of ASDs (with same manufacturing method) in regards of crystallization onset based on a few fast measurements, even accounting for the influence of different crystallinity levels (e.g. different detection levels of different analytical techniques).

2. Materials and methods

ASDs were prepared by spray drying and treated by secondary drying to remove residual solvent. PVPVA (Plasdone S-630) and Soluplus® were used as polymers and were obtained from Ashland Inc. (Columbus, USA) and BASF SE (Ludwigshafen, Germany), respectively. Griseofulvin (GRI) (Ph. Eur. Grade) was investigated as model API and was purchased from Fagron (Rotterdam, Netherlands). Dichloromethane (purity >98%) served as solvent in the spray-drying process and was purchased from VWR (Randor, USA). All substances were used without further purification.

Crystallinity measurements were performed using water-sorption measurements and Raman measurements. Filtered and deionized water (Merck Millipore purification system, Darmstadt, Germany) was used for generating water vapor in the DVS/crystallinity measurements and shelf life tests. A detailed description of the applied methods is provided in part 1 of this paper series (Wolbert et al., 2022a).

3. Modeling

3.1. Extension of Johnson-Mehl-Avrami-Kolmogorov model with classical nucleation theory

The crystallization kinetics were described using one of the most commonly applied empirical models for crystallization kinetics – the JMAK model (Avrami, 1939; Avrami, 1940). The JMAK model simplifies the crystallization process by assuming homogeneous nucleation and time-independent nucleation rates and crystal-growth rates. Due to the assumption of homogeneous nucleation, the JMAK model is sensitive to the number of growing nuclei and their volume fraction. Todinov (Todinov, 2000) showed that the crystallized API fraction calculated by the JMAK equation is quite precise at a high nuclei number but deviates significantly from experimental studies for a small number of nuclei (Todinov, 2000). The original JMAK equation was derived from a volume balance. Assuming that the crystalline API, the amorphous API, and the polymer have the same density, the following mass-related Eq. (1) was used to determine the crystallinity α over the time t (Yang et al., 2010; Avrami, 1939; Avrami, 1940):

$$\alpha(t) = 1 - exp(-k\cdot(t-\tau)^n) \text{ with } \alpha = \frac{m_{API}^S}{m_{API}^F} \quad (1)$$

The crystallinity α is defined in this work as the mass ratio of crystalline API in the ASD m_{API}^S to the total mass of API in the ASD formulation m_{API}^F. τ describes the crystallization onset point (set to zero if nucleation occurs spontaneously, statistical nucleation inhibition is not considered and the predicted onset time thus corresponds to the worst-case scenario), k is the crystallization-rate constant, and n describes the dimensionality of the crystal growth – the Avrami exponent. (Yang et al., 2010; Avrami, 1939; Avrami, 1940) GRI crystallizes in the form of needles, leading to $n = 2$ (Wolbert et al., 2022a; Zhou et al., 2008). For $t < \tau$, α is defined as zero.

According to the derivation of the JMAK equation, the crystallization-rate constant k describes the nucleation as well as the seed growth in the corresponding spatial directions of the crystal. Since GRI exhibits needle-like growth, the crystals increase their size only in one spatial direction by the growth rate. Accordingly, the crystallization-rate constant k linearly depends on the crystal-growth rate $\dot{G}$ and the nucleation rate $\dot{N}$ (Eq. (2)).

$$k = \dot{N}\cdot\dot{G} \quad (2)$$

To predict the shelf life in terms of crystallization onset in ASDs, the empirical JMAK equation was combined with the classical nucleation theory (Mullin, 2001; *Nucleation Theory*, 2013). According to the classical nucleation theory (Mullin, 2001; *Nucleation Theory*, 2013), nucleation and crystal growth are distinct mechanisms during crystallization. The classical expression for the nucleation rate $\dot{N}$ of spherical crystal nuclei is shown in Eq. (3) (Christian, 2003; Andronis and Zografi, 2000).

$$\dot{N} = A\cdot\frac{T}{\eta}\cdot exp\left[-\frac{16\pi\sigma^3}{3\,k_B T\Delta G^2}\right] \quad (3)$$

Herein, A is a constant, η is the viscosity, σ the crystal-amorphous interfacial energy, ΔG the change in Gibbs free energy per unit volume for the transformation from the amorphous to the crystalline state, and k_B is the Boltzmann constant. In a multi-component mixture, the difference in Gibbs free energy depends on the intermolecular interactions among the molecules and on the thermodynamic supersaturation $ln(S)$ (Eq. (4)) (Tung et al., 2009; Andronis and Zografi, 2000).

$$\Delta G = k_B\cdot T\cdot ln(S) \text{ with } ln(S) = ln\left(\frac{a_{API}}{a_{API,eq.}}\right) = ln\left(\frac{\gamma_{API}^L\cdot x_{API}^L}{\gamma_{API,eq.}^L\cdot x_{API,eq.}^L}\right) \quad (4)$$

The supersaturation is defined as the logarithm of the ratio of API thermodynamic activity in the initially fully amorphous ASD (a_{API}) and

the thermodynamic activity of the API in the equilibrium-crystallized ASD ($a_{API,eq.}$). The thermodynamic activity is defined as the product of the mole fraction of the API x^L_{API} and its activity coefficient γ^L_{API}in the amorphous ASD (phase L). The thermodynamic activity in the equilibrium-crystallized ASD is obtained from the equilibrium Eq. (5).

$$a_{API,eq} = \gamma^L_{API,eq} \cdot x^L_{API,eq} = exp\left(-\frac{\Delta h^{SL}_{API}}{RT}\left[1-\frac{T}{T^{SL}_{API}}\right] - \frac{\Delta c^{SL}_{p,API}}{R}\left[ln\left(\frac{T^{SL}_{API}}{T}\right) - \frac{T^{SL}_{API}}{T} + 1\right]\right) \quad (5)$$

It depends on the APIs' melting enthalpy Δh^{SL}_{API}, melting temperature T^{SL}_{API} and the difference in heat capacities of liquid and solid API $\Delta c^{SL}_{p,API}$.The activity coefficient γ^L_{API} accounts for intermolecular interactions between the API and all other molecules (here polymer and water). This activity coefficient is calculated using PC-SAFT (see Section 3.2). R is the universal gas constant (8.314 J/mol/K). The method of describing the interplay between crystallization equilibrium and moisture sorption needs to be considered for correctly estimating S as described in the first part of this paper series (Wolbert et al., 2022a).

Combining Eqs. (3) and (4) results in the final expression for the nucleation rate (Eq. (6)).

$$\dot{N} = A \cdot \frac{T}{\eta} \cdot exp\left[-\frac{16\pi\sigma^3}{3 \cdot k_B^3 \cdot T^3 \cdot (ln(S))^2}\right] = A \cdot \frac{T}{\eta} \cdot exp\left[\frac{-B}{T^3 \cdot (ln(S))^2}\right] \quad (6)$$

It is assumed that for a given API/polymer combination, σ is constant. The constants in the argument of the exponential function were combined into one single constant B. The viscosity was calculated applying the approach of Wolbert et al (Wolbert et al., 2020). based on the WLF equation (Williams et al., 1955; Williams and Ferry, 1954) (Section 3.4), and the supersaturation was obtained from PC-SAFT (Section 3.2).

The classical expression for crystal growth is shown in Eq. (7) (Andronis and Zografi, 2000; Gutzow, 1977), whereas C is a constant.

$$\dot{G} = C \cdot \frac{T}{\eta} \cdot \left(1 - exp\left[-\frac{\Delta G}{k_B \cdot T}\right]\right) \quad (7)$$

Eq. (7) is further simplified using Eq. (4) to Eq. (8).

$$\dot{G} = C \cdot \frac{T}{\eta} \cdot \left(1 - \frac{1}{S}\right) \quad (8)$$

Thus, also crystal growth is a function of viscosity η and supersaturation ln(S). Combining Eqs. (6) and (8) results in the following expression for the crystallization-rate constant k (Eq. (9)):

$$\mathrm{k} = \dot{G} \cdot \dot{N} = k' \cdot \left(\frac{T}{\eta}\right)^2 \cdot \left(1 - \frac{1}{S}\right) \cdot exp\left[\frac{B}{T^3 \cdot (ln(S))^2}\right] \quad (9)$$

All values that are constants or only depend on the particular API/polymer combination were summarized in k' and B. They were fitted to experimentally determined k values and were assumed not to depend on viscosity neither on supersaturation. Once k' and B have been determined by fitting to fast and convenient measurements, they were used to predict the crystallization kinetics of the same API/polymer combination at different storage conditions and/or different drug loads.

3.2. PC-SAFT

The thermodynamic activities of the API, polymer and water were predicted in this work using PC-SAFT. PC-SAFT calculates the residual Helmholtz energy a^{res} as the sum of different contributions (Eq. (10)) (Gross and Sadowski, 2001).

$$a^{res} = a^{hc} + a^{disp} + a^{assoc} \quad (10)$$

Molecules are considered as repulsive (hard) chains a^{hc} of m^{seg} spherical segments with diameter σ. The contribution of attractive van-der-Waals forces is described by a^{disp} and the contribution of associative forces, like the formation of hydrogen bonds between associating molecules, is covered by a^{assoc}. Non-associating molecules are characterized by three pure-component parameters: the segment number m^{seg}, segment diameter σ and the dispersion-energy parameter $\frac{u}{k_B}$ (k_B being the Boltzmann constant), which describes the attraction potential between two molecules.

Associating molecules require five pure-component parameters: the three parameters mentioned before as well as the association volume κ^{AB} and the association-energy parameter $\frac{\varepsilon^{AB}}{k_B}$. The pure-component parameters of all substances considered in this work were taken from literature and are listed in Table 1.

The segment diameter and the dispersion energy in mixtures were described according to Berthelot-Lorentz mixing rules (Calvin and Reed, 1971), and cross association between unlike molecules was described according to Wolbach and Sandler (Wolbach and Sandler, 1998). A binary interaction parameter k_{ij} between two components i and j is used to correct the dispersion-energy contribution in mixtures (Eq. (11)).

$$u_{ij} = \left(1 - k_{ij}\right)\sqrt{u_i \cdot u_j} \quad (11)$$

The binary interaction parameters k_{ij} were taken from literature and are summarized in Table 2.

3.3. Calculation of glass-transition temperatures

The glass-transition temperature of the ASD ($T_{g,ASD}$) was estimated applying the Gordon-Taylor approach. The glass-transition temperature depends on the composition of the ASD, here employing the weight fractions of the components i (w_i), as well as the glass-transition temperatures of the pure components i ($T_{g,i}$) in Kelvin (Eq. (12)) (Gordon and Taylor, 1952).

$$T_{g,ASD} = \frac{\sum_i K_i \cdot w_i \cdot T_{g,i}}{\sum_i K_i \cdot w_i} \quad (12)$$

According to the Simha-Boyer rule (Simha and Boyer, 1962) (Eq. (13)), the parameters K_i weigh the influence of each component on the glass-transition temperature based on the densities (ρ_i) and glass-transition temperatures.

$$K_i = \frac{\rho_{polymer} \cdot T_{g,Polymer}}{\rho_i \cdot T_{g,i}} \quad (13)$$

Table 1 lists the glass-transition temperatures and densities of all components investigated in this work.

3.4. Calculating the viscosity of ASDs

As shown in a previous work (Wolbert et al., 2020) (Wolbert et al., 2020), an apparent temperature can be used to account for the influence of the API (here GRI) and of water on the viscosity of ASDs (Wolbert et al., 2020; Mueller et al., 2010). The apparent temperature ($T_{apparent}$) considers the decrease of $T_{g,ASD}$ due to the API incorporation in the ASD matrix and due to water sorption relative to the glass-transition temperature $T_{g,polymer}$ of the pure polymer (Eq. (14)).

$$T_{apparent} = T + \left(T_{g,polymer} - T_{g,ASD}\right) \quad (14)$$

The glass-transition temperature of the ASD ($T_{g,ASD}$) is calculated using the Gordon-Taylor equation (Section 3.3).

3.4.1. Calculating the viscosity of ASDs above T_g

The Williams-Landel-Ferry (WLF) equation describes the temperature dependence of polymer viscosities in the range $\left(T_g - 10K\right) \langle T < \left(T_g + 100K\right)$ (Osswald and Rudolph, 2014). In this work, the zero-shear-viscosity η_0 is used resulting in Eq. (15) (Williams et al., 1955; Ferry, 1980).

Table 1
PC-SAFT pure-component parameters and the glass-transition temperatures and amorphous densities of all components investigated in this work.

	M/	$\frac{m^{seg}}{M}$/	σ/	$\frac{u}{k_B}$/	$\frac{\varepsilon^{AB}}{k_B}$/	κ^{AB}	N^{assoc}	T_g /	ρ/
	g/mol	mol/g	Å	K	K			°C	g/cm^3
GRI	352.77	0.0402 (Paus et al., 2015)	3.372 (Paus et al., 2015)	221.261 (Paus et al., 2015)	1985.49 (Paus et al., 2015)	0.02 (Paus et al., 2015)	2/2 (Paus et al., 2015)	87.75 (Paus et al., 2015)	1.42 (Zhou et al., 2008)
PVPVA	47,000	0.0372 (Lehmkemper et al., 2017)	2.947 (Lehmkemper et al., 2017)	205.271 (Lehmkemper et al., 2017)	0 (Lehmkemper et al., 2017)	0.02 (Lehmkemper et al., 2017)	472/472 (Lehmkemper et al., 2017)	108.05 (Six et al., 2004)	1.19 (Six et al., 2004)
Soluplus®	118,000	0.0540 (Wolbert et al., 2022b)	2.809 (Wolbert et al., 2022b)	225.000 (Wolbert et al., 2022b)	0 (Wolbert et al., 2022b)	0.02 (Wolbert et al., 2022b)	2486/2486 (Wolbert et al., 2022b)	68.40 (Rask et al., 2018)	1.14 (Rask et al., 2018)
PVAc	90,000	0.0321 (Tumakaka et al., 2002)	3.397 (Tumakaka et al., 2002)	204.650 (Tumakaka et al., 2002)	0 (Wolbert et al., 2020)	0.02 (Wolbert et al., 2020)	1047/1047 (Wolbert et al., 2020)	43.68 (Prudic et al., 2014)	1.18 (Jelinska et al., 2010)
water	18.015	0.0669 (Cameretti and Sadowski, 2008)	σ_{water} [#]	353.945 (Cameretti and Sadowski, 2008)	2425.67 (Cameretti and Sadowski, 2008)	0.0451 (Cameretti and Sadowski, 2008)	1/1 (Cameretti and Sadowski, 2008)	−135.15 (Hallbrucker et al., 1989)	1.00

[#] $\sigma_{water} = 2.7927 + 10.11\ \exp.(-0.01775 \cdot T/K) - 1.417 \cdot \exp.(-0.01146 \cdot T/K)$ (Cameretti and Sadowski, 2008).

Table 2
PC-SAFT binary interaction parameters (k_{ij}) between compounds investigated in this work.

	k_{ij}
GRI / PVPVA	−0.0041 (Wolbert et al., 2022b)
GRI/ Soluplus®	−0.0066 (Wolbert et al., 2022b)
GRI/PVAc	0.0010 (Wolbert et al., 2022a)
GRI/ water	0.0125 (Wolbert et al., 2022b)
water / PVPVA	−0.1565 (Lehmkemper et al., 2017)
water / Soluplus®	−0.0780 (Wolbert et al., 2022b)
water/PVAc	−0.1313 (Wolbert et al., 2020)

$$log\frac{\eta_0}{\eta_{0,ref}} = loga_T = \frac{-c_1(T - T_{ref})}{c_2 + T - T_{ref}} \quad (15)$$

η_0 and $\eta_{0,ref}$ denote the zero-shear-viscosity at measurement temperature T and reference temperature T_{ref}, respectively. The shift factor a_T accounts for the temperature change, c_1 and c_2 are polymer-specific constants that depend on T_{ref} (). The constants c_1 and c_2 used in this work were taken from a previous work and literature (PVPVA) (Wolbert et al., 2020; Bochmann et al., 2016) or fitted to experimental data (Soluplus, fit shown in SI).

The temperature in Eq. (15) was replaced by the apparent temperature (Eq. (14)) to account for the influence of API and of water on ASD viscosity, resulting in Eq. (16).

$$log\frac{\eta_0}{\eta_{0,ref}} = loga_T = \frac{-c_1(T_{apparent} - T_{ref})}{c_2 + T_{apparent} - T_{ref}} \quad (16)$$

Table 3: lists the WLF constants c_1 and c_2 for PVPVA and Soluplus with their reference temperature and reference viscosity. Details of the method are described in our previous publication (Wolbert et al., 2020).

3.4.2. Calculating the viscosity of ASDs below T_g

The temperature dependency of polymer viscosity in the range $T < (T_g - 20K)$ is described in this work using the linearized form of the Arrhenius equation as a function of the apparent temperature introduced earlier(Greco et al., 2012; Osswald and Rudolph, 2014). The viscosity of the ASD is determined as follows in Eq. (17).

$$ln(\eta_0) = \frac{-E_A}{R}\cdot\frac{1}{T_{apparent}} + ln(A) \quad (17)$$

E_A is the relaxation activation energy, R is the universal gas constant and A is a temperature-independent constant only depending on the API/polymer system.

Due to the linear expression of the Arrhenius equation, two viscosities of the ASD in the validity range of the Arrhenius equation are sufficient to fit the activation energy and the ln(A) value. As previously described, the WLF equation loses its validity at temperatures less than about 10 K below the glass transition temperature. Therefore, (T_g - 10 K) was chosen as the intersection of the WLF and Arrhenius equations and the viscosity at this temperature was determined using the WLF equation. The fastest crystallization-kinetics measurement in the validity range of the Arrhenius equation was used to determine the second viscosity to determine ln(A) and E_A.

The activation energy values and $ln(A)$ values determined in this work for the two ASD combinations (GRI/PVPVA and GRI/Soluplus) are shown in Table 4. Since in a temperature range between $T_g > T > (T_g - 20K)$ structural relaxation (often also referred to as physical aging) can occur, the Arrhenius parameters are only valid at temperatures below $(T_g - 20K)$. Flügel et al. (2020) have proven that annealing of PVPVA at temperatures between the glass-transition temperature and 13 K below the glass-transition temperature, significantly affects the mechanical properties of the material (e.g. the relaxation enthalpy peak at T_g, the Young's modulus, or the tensile strength).

Table 4
Activation energy for relaxation E_A and the constant $ln(A)$ for GRI/PVPVA and GRI/Soluplus ASDs determined in this work.

API/Polymer	-E_A/R	ln(A) T < (T_g - 20 K)
GRI/PVPVA	12,141	−9.10
GRI/Soluplus	9849	−3.40

Table 3
WLF model parameters c_1 and c_2 for PVPVA and Soluplus® with their reference temperature and reference viscosity.

Polymer	c_1/ -	c_2/ °C	T_{ref}/ °C	$\eta_{0,ref}$/ Pa·s
PVPVA	10.04 (Bochmann et al., 2016)	147.40 (Bochmann et al., 2016)	150 (Bochmann et al., 2016)	61,006 (Bochmann et al., 2016)
Soluplus®	19.16*	243.27*	100*	29,355,600*

* This work.

4. Results and discussion: Procedure for predicting the shelf life

The shelf life was calculated as described in the previous section using Eq. (9) and Eq. (1). For this calculation, the supersaturation, the viscosity, and the fitting parameters k' and B (which only depend on the particular API/polymer combination) were required. Fig. 1 shows the modeling approach developed in this work including the sub models/ building blocks and how they are linked to predict the shelf life of ASDs with regards to crystallization onset.

According to this scheme, first the API/polymer combination of interest was selected, and a manufacturing method was chosen. GRI/PVPVA and GRI/Soluplus were selected for this study and the ASDs were manufactured via spray drying. A detailed description of the manufacturing method and the phase diagrams of the selected ASDs are provided in Part 1 of this work (Wolbert et al., 2022a). The model parameters k' and B were fitted to experiments performed at accelerated conditions and then used in a second step to predict the shelf life at storage conditions.

4.1. Model-parameter fitting at accelerated conditions

Starting at the left side of Fig. 1, the first step is the prediction of the water absorption in the ASD (here: GRI/PVPVA and GRI/Soluplus) at accelerated conditions using PC-SAFT (see Table 6). Knowing the amount of water absorbed by the ASD, the supersaturation of the API in the ASD is then determined (again using PC-SAFT – see Part 1 (Wolbert et al., 2022a). When determining the supersaturation, it should be checked whether a moisture-induced miscibility gap forms in the ASD (e.g. by means of PC-SAFT). In that case, the concentrations of API and polymer differ significantly in the two phases, which leads to a different supersaturation than in the non-demixed ASD. Moreover, crystallization kinetics might overlap with demixing kinetics.

Secondly the glass-transition temperature of the wet ASD was calculated using the Gordon-Taylor equation (Eq. (12)). As demonstrated in a previous work, the Gordon-Taylor equation aptly describes the glass-transition temperature of the ASDs investigated in this work (Wolbert et al., 2022b). The glass transition temperature was then used to calculate the apparent temperature (Eq. (14)), which was used for the viscosity models. As third step, the viscosity of the ASD at accelerated conditions is estimated using the WLF equation and the procedure already presented and validated in our previous work (see Wolbert et al., 2020 and SI) as described in Section 3.4.1. As fourth step, fast crystallization-kinetics measurements above the glass-transition temperature of GRI/PVPVA ASDs and GRI/Soluplus ASDs were performed to determine the GRI crystallization rate constants ln(k) (see Table 6). For a detailed description of the measuring method, we refer to the Part 1 of this work (Wolbert et al., 2022a). Finally, the model parameter k' and B were fitted to the experimentally determined ln(k) values using Eq. (9), the viscosity above the glass transition determined via the WLF equation (Section 3.4.1), and the supersaturation determined via PC-SAFT (Section 3.2). As described above, the model parameters k' and B are considered to be generally valid for a specific API/polymer system

Table 5
Fitted model parameters k' and B for GRI/PVPVA ASDs and GRI/Soluplus ASDs.

API/Polymer	k'	B
GRI/PVPVA	$4.65 \cdot 10^{17}$	$4.16 \cdot 10^{9}$
GRI/Soluplus	$2.06 \cdot 10^{15}$	$2.18 \cdot 10^{9}$

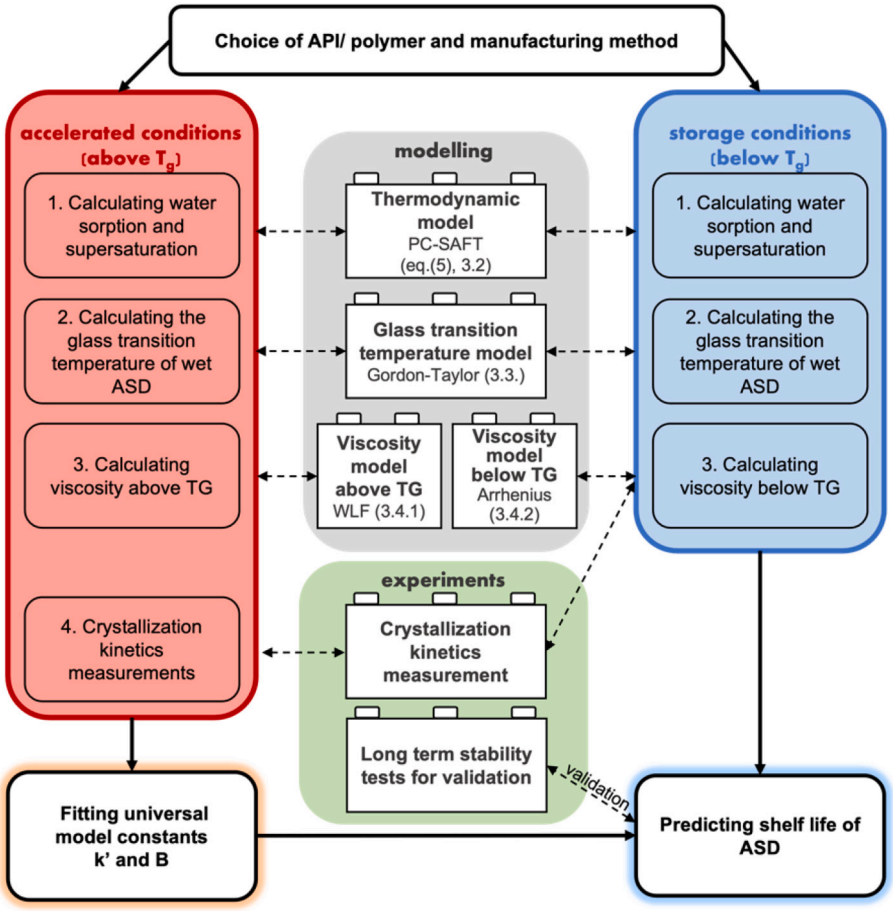

Fig. 1. Scheme for predicting the shelf life (crystallization onset) of ASDs.

and manufacturing method. Table 5 shows the values k' and B obtained for the systems GRI/PVPVA and GRI/Soluplus ASDs.

4.2. Shelf-life prediction at storage conditions

At the right side of Fig. 1, the shelf life prediction at storage conditions (here 25 °C/ 60% RH and 25 °C/ 10% RH) is described. The first and second step at storage conditions are the same as for accelerated conditions. First, the water sorption in the ASD and supersaturation of the API were predicted with PC-SAFT and second, the glass-transition temperature and the apparent temperature of the wet ASD at the conditions of interest were calculated.

The viscosity calculation in the third step is different at storage conditions since the WLF equation is not valid at temperatures lower than about 10 K below the glass-transition temperature. Therefore, the Arrhenius equation was used to calculate the viscosity below glass-transition temperature (Section 3.4.2).

4.2.1. Estimation of the Arrhenius parameters

The determination of the viscoelastic behavior below the glass-transition temperature is very challenging, time-consuming, thermal-history dependent and little data is available for commonly used polymers or APIs. Due to the linear expression of the Arrhenius equation, two measurements of the ASD viscosity in the validity range of the Arrhenius equation are sufficient for fitting the parameters. Viscosity measurements below the glass-transition temperature would be possible e.g. via DMA. As the thermal history of those samples completely differs from the one of a spray-dried powder, the so-obtained values would also completely differ from those of the spray- dried material.

Therefore, in this work, the viscosity of the ASD at the intercept between the WLF and Arrhenius equation (at T_g – 10 K) was calculated using the WLF equation. Additionally, one crystallization-kinetics measurement below the glass-transition temperature (the one with the highest drug load at 25 °C/ 60 RH, as this was always the fastest) was performed and the resulting ln(k) value was inserted into the modeling approach developed in this paper (Eq. (9)) to calculate the viscosity using the before-hand determined model parameters k' and B.

Using the intercept and the viscosity calculated from the single crystallization-kinetics measurement, the Arrhenius parameters (the activation energy (E_A) and ln(A) values) were obtained. This approach ensures considering the thermal history of the spray-dried powder. Once the Arrhenius parameters are determined for a specific ASD, they can be used for any API load, temperature, and RH.

Fig. 2 shows the two models (WLF and Arrhenius) used to describe the viscosity of ASDs in this work and their respective validity ranges. To validate the viscosity models the crystallization-kinetics measurements, the model parameters k' and B and Eq. (9) were used to calculate the viscosities of the ASDs of interest (symbols in Fig. 2). It can be seen that at the glass-transition temperature ($T_g/T_{apparent}$ = 1) and above, the viscosities calculated from the crystallization kinetics follow the WLF equation. Below about 20 K below the glass-transition temperature ($T_g/T_{apparent}$ > 1.07), the Arrhenius approach describes the viscosities very well.

As can be seen in Fig. 2, there are some viscosities slightly below the glass-transition temperature (up to about $T_g/T_{apparent}$ = 1.07) that cannot be described by the Arrhenius equation (light blue symbols). The reason is the structural relaxation in these samples stored close to the glass-transition temperature (see Section 3.4.2). However, this phenomenon is not important for predicting the shelf life of ASDs. Practically relevant ASDs are stored far below the glass-transition temperature and produced with fast cooling rates (e.g., manufacturing via spray drying), therefore, structural relaxation will never occur in these ASDs. To avoid an influence of structural relaxation on the modeling and shelf-life predictions, the Arrhenius parameters were fitted to the intercept with the WLF equation and the fastest crystallizing ASDs which were stored at 25 °C and 60% RH (red star). All other ASDs stored at 25 °C and 60% RH and 25 °C and 10% RH (see dark blue symbols in Fig. 2) are also well described by the Arrhenius equation using the same parameters as before.

This means, once the Arrhenius parameters are determined, viscosities of ASDs stored below their glass-transition temperature can be indirectly determined from crystallization-kinetics measurements. This also provides an estimation method for the viscosity of highly supercooled, thermodynamically metastable ASDs, which is impossible or time-consuming to measure when applying conventional direct viscosity measurements (Flügel et al., 2020).

4.2.2. Shelf-life prediction

After all steps have been performed at storage conditions, the shelf life of the ASDs can be predicted using the supersaturation, viscosity, temperature, and the model parameters k' and B beforehand determined at accelerated conditions. The crystallization-rate constants ln(k) were finally calculated using Eq. (9). Fig. 3 shows contour plots of the crystallization-rate constants ln(k) as a function of supersaturation and viscosity for the systems investigated in this work. Measurements were performed between 40 °C and 85 °C to fit the model parameters, which were then used to predict the crystallization rate at 25 °C.

The contour plots in Fig. 3a and Fig. 3c show the ln(k) values above the glass-transition temperature to which k' and B have been fitted – these measurements were performed at 40 °C - 85 °C and at different RHs. It can be seen that the colour of the symbols perfectly matches the colour of the diagram – which means that the crystallization kinetics (ln (k) values) of the ASDs stored at different temperatures (above T_g), RHs and drug loads can be accurately reproduced using the k' and B values fitted to this data. Using the so-determined parameters k' and B (Table 5), the contour plots were predicted for 25 °C (Fig. 3b and Fig. 3d) (this can of course also be done for any other temperature).

The contour plots in Fig. 3b and Fig. 3d indicate states that are

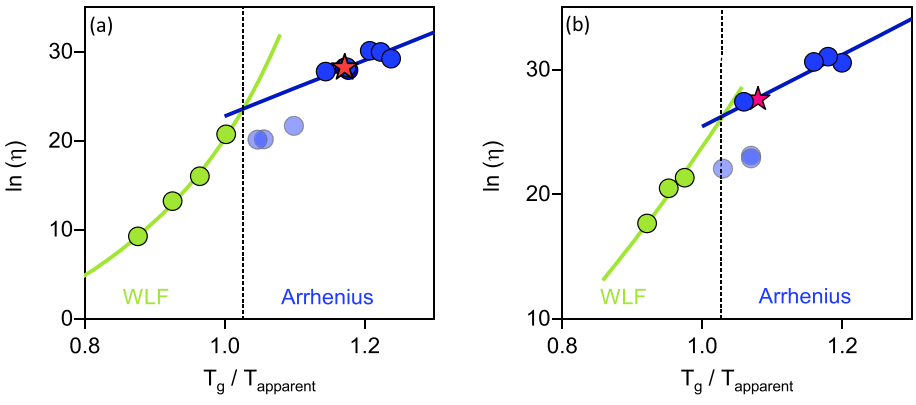

Fig. 2. Viscosity as function of the ratio of the glass-transition temperature and the apparent temperature ($T_g/T_{apparent}$) of a) GRI/PVPVA ASDs and b) GRI/Soluplus ASDs. The green lines show the WLF model, the blue line indicates the Arrhenius model. Green symbols represent ASDs stored above the glass-transition temperature, light blue symbols represent ASDs stored between the glass-transition temperature and about 20 K below the glass-transition temperature and the dark blue symbols represent ASDs stored at an even lower temperature. The Arrhenius parameters were determined using the intercept between the WLF and Arrhenius equation (at T_g – 10 K) and the viscosity of the fastest crystallizing ASD below T_g (red star). (For interpretation of the references to colour in this figure legend, the reader is referred to the web version of this article.)

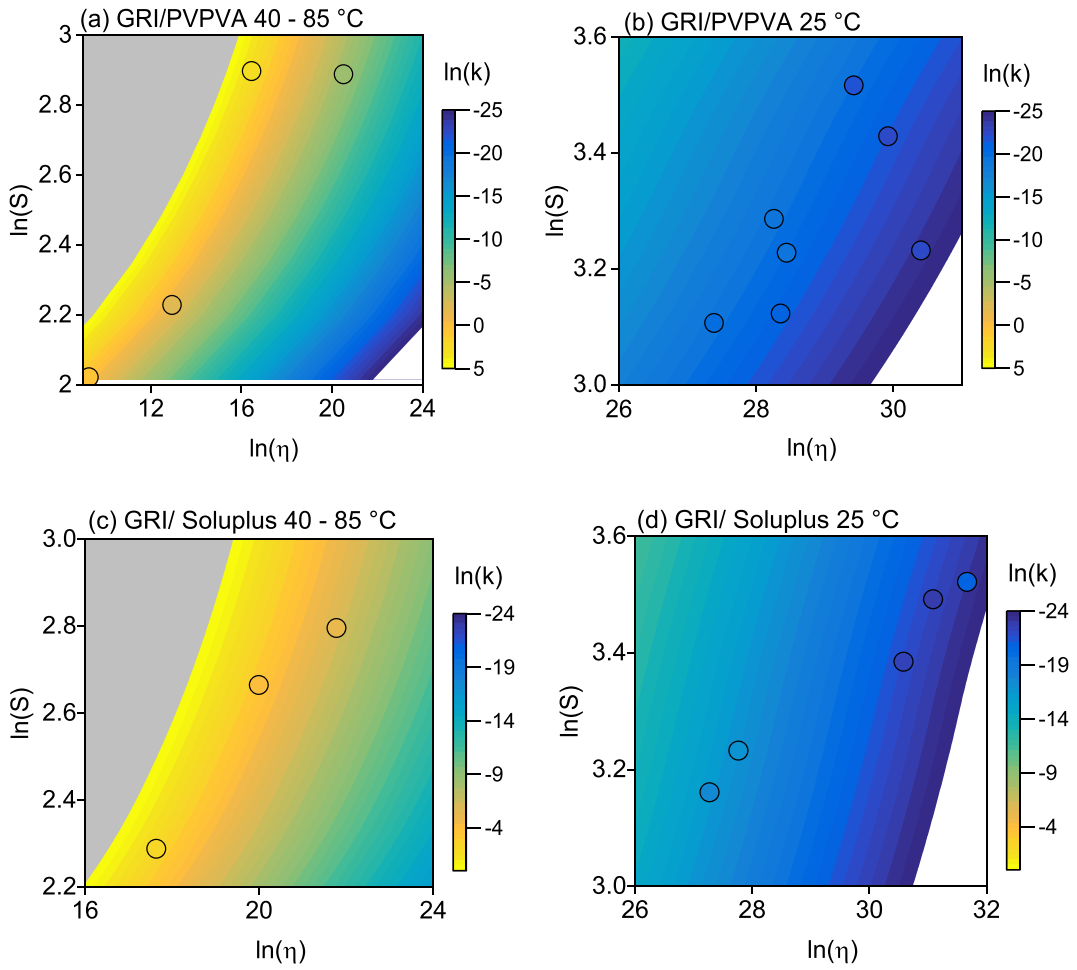

Fig. 3. Contour plots showing the dependency of the crystallization-rate constant ln(k) on supersaturation (S) and viscosity (η). ln(k) is colour coded as indicated next to the diagrams. The position of the symbols indicates the ln(k) values predicted using the approach presented in this work (see Table 6 and Table 7), whereas the colour of the symbols indicates the ln(k) value experimentally obtained from the crystallization-kinetics measurements (see Table 6 and Table 7). A perfect match of prediction and measurement is found when the colour of the symbol matches the colour of the diagram at the position of the symbol. (a) GRI/PVPVA ASDs at 40 °C - 85 °C, (b) GRI/PVPVA ASDs at 25 °C, (c) GRI/Soluplus ASDs at 40 °C - 85 °C and (d) GRI/Soluplus ASDs at 25 °C.

located below the glass-transition temperature. The symbols again represent the ln(k) values determined via long-term crystallization-kinetics measurements at 25 °C / 60% RH and 25 °C/ 10% RH. As can be seen, the colours of the symbols (measured ln(k)) fit very well with the position in the diagram – meaning we were able to predict the ln(k) values (and therewith the shelf life) of the ASDs stored at 25 °C at different RHs and with different API loads. This proves our assumption that once k' and B have been determined for an ASD produced using a defined manufacturing method, they can be used to predict the shelf life of this ASD at any other condition of interest.

Using the ln(k) values, the shelf life of the ASDs was calculated via the JMAK equation. The latter provides the time it takes to reach a certain degree of crystallization (the shelf life). To compare the predicted shelf life to our crystallization-kinetics measurements, we choose a degree of crystallization of 5% (alpha in the JMAK Eq. (1)) as the level of detection of our PXRD device is about 5% crystallinity. Table 6 and Table 7 show the measured and predicted shelf life (5% crystallinity) at the specified storage conditions (temperature and relative humidity) of the ASDs investigated in this work.

Table 6 shows the results of the crystallization-kinetics

Table 6
API/ polymer combination, drug load of dry ASD, and the measured and predicted shelf life (5% crystallinity) and the distance to the glass-transition temperature at storage conditions (temperature and RH) of the ASDs stored at or above glass transition. (p – m) is the deviation between the predicted (p) and measured (m) shelf life. Crystallization kinetics measured via Raman spectroscopy.

API/ Polymer	T / °C	RH / %	drug load	(T – T_g)/ K	measured shelf life / min	predicted shelf life / min	(p – m) /min
GRI/ PVPVA	85	60	0.4	31	53	38	−15
	85	60	0.2	54	28	27	−1
	40	75	0.6	−1	318	231	−87
	40	75	0.4	14	5	7	−2
GRI/ Soluplus	50	75	0.4	9	286	433	+147
	60	75	0.4	17	190	115	−75
	85	60	0.4	29	59	66	+7

Table 7
ASDs, drug load of dry ASD, and the measured and predicted shelf life (5% crystallinity) and the distance to the glass-transition temperature at storage conditions (temperature and RH) of the ASDs stored below glass transition. The measured shelf life is given as time interval between two measurements: the last one at which no crystals have been detected and the one at which crystals have been detected for the first time.(p − m) is the distance of the predicted (p) shelf life from the measured (m) shelf-life interval. If the predicted shelf life lies with the measured shelf-life interval, the distance is zero. *The ASDs did not crystallize until the end of the observation period (33 months).

API/ Polymer	T / °C	RH / %	drug load	T – T_g / K	measured shelf life / month	predicted shelf life / month	(p − m) /months
GRI/ PVPVA	25	60	0.80	−56	4.2–4.7	4.5	0.0
	25	60	0.60	−57	4.5–5.6	8.1	+2.5
	25	60	0.40	−57	12.0–16.8	15.4	0.0
	25	60	0.20	−48	12.0–16.8	9.5	−2.5
	25	10	0.80	−66	13.9–15.4	7.1	−6.8
	25	10	0.60	−70	15.9–26.7	19.0	0.0
	25	10	0.40	−73	26.7–32.5	92.1	+25.5
	25	10	0.20	−77	>33*	3171.3	–
GRI/ Soluplus	25	60	0.40	−24	1.5–2.1	1.8	0.0
	25	60	0.20	−20	2.9–4.8	3.0	0.0
	25	10	0.8	−56	11.7–15.7	25	+9.6
	25	10	0.60	−52	23.3–32.7	28	0.0
	25	10	0.40	−48	23.3–33.0	28	0.0
	25	10	0.20	−45	>33*	42	–

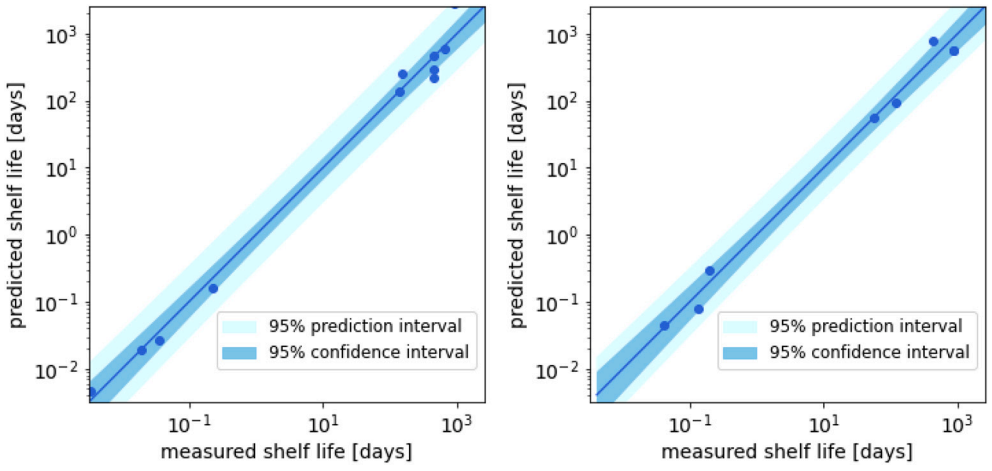

Fig. 4. Comparison of predicted and measured ASD shelf life (5% crystallinity) of a) GRI/PVPVA and b) GRI/Soluplus ASDs. The blue solid line represents the line of perfect agreement between the predicted and measured shelf life values. The blue symbols represent the measured shelf life of ASDs stored above (values of Table 6) and far below the glass-transition temperature (mean value of the shelf-life intervals from Table 7) and the vertical distances between the symbols and the blue line represents the deviations between the measured and predicted shelf life values. The dark blue area is the 95% confidence interval and the light blue area is the 95% prediction interval. (For interpretation of the references to colour in this figure legend, the reader is referred to the web version of this article.)

measurements (at and above the glass-transition temperature) to which the parameters k' and B were adjusted. Table 7 shows the results of the long-term crystallization-kinetics measurements of the ASDs stored far below the glass-transition temperature (20 K to 77 K below T_g). It should be noted that the crystallization onset is given in minutes in Table 6 and in months in Table 7. This illustrates that within a few hours to a few weeks, the crystallization-kinetics measurements can be performed for parameter estimation (Table 6 and fastest measurement of Table 7 for determining k' and B and the Arrhenius parameters, respectively), which then can be used to predict the onset of crystallization in ASDs over time intervals of several years (Table 7).

Further, Table 7 shows that even storage at 50 K below the glass-transition temperature does not protect the ASDs from crystallization. For example, the GRI/PVPVA ASD with a drug load of 40 wt% stored at 25 °C and 10% RH (-73 K below T_g) crystallized between 26.7 and 32.5 months. Deviations between measured shelf life and predicted one partly result from the fact that due to the long-term nature of the measurements (over approx. 3 years), some of the measurements are only single measurements. Moreover, the measurement intervals became longer over time (see Table 7). However, given these uncertainties in the measured crystallization kinetics, it is even more remarkable that the shelf life predicted always yields the correct order of magnitude. Fig. 4 illustrates this very well showing the comparison of predicted and measured shelf life (values of Table 6 and Table 7 (mean of intervals)) on a logarithmic scale. In addition, Fig. 4 shows the 95% confidence interval (CI) and prediction interval (PI) referring to the predicted shelf-life values obtained from the model. The 95% confidence intervals (CI) indicate the range in which the true mean shelf life is expected to lie with 95% confidence. The 95% prediction intervals (PI) show the range of values in which individual future measurements of the shelf life are expected to lie with 95% probability. The narrower the confidence and prediction intervals, the more precise the model predictions of the shelf life of ASDs.

Fig. 4 compares the experimentally determined shelf life (crystallinity detected in our long-term studies via PXRD (Wolbert et al., 2022b)) and the predicted shelf life and therewith the quality of the prediction. As already mentioned above, it can be seen that the predicted and observed shelf life are always in the same order of magnitude and therefore agree very well. This is even more remarkable as the experimental data were taken at different storage temperatures, different storage relative humidities, and different API loads (see Table 6 and Table 7). In Fig. 4a the MAPE (Mean Absolute Percentage Error) for GRI/PVPVA is 7.6% and the R^2 is 98.1% and in Fig. 4b the MAPE for GRI/Soluplus is 13.7% and the R^2 is 94.2%.

5. Conclusion

In this paper, we proposed an approach to predict the shelf life (crystallization onset) of ASDs. Our special focus was to deduce the complexity of the model equations and to minimize the number of

required parameters to ensure applicability in ASD development.

It was shown that (fast) crystallization-kinetics measurements above the glass-transition temperature could be used to fit universal model parameters. These model parameters are specific for an API/polymer combination and a given manufacturing method and do also apply to other API loads and storage conditions (temperature, RH). Besides the model parameters, only the supersaturation of the ASD, the viscosity of the pure polymers above the glass transition and the viscosity of the ASD below the glass transition are required to predict the crystallization kinetics (shelf life) of the ASD. In this work, the supersaturation was calculated using PC-SAFT. The viscosity of ASDs was modeled using the WLF model for temperatures above the glass transition of the wet ASD and the Arrhenius equation for temperatures below the glass transition. To fit the Arrhenius parameters one additional crystallization-kinetics measurement below the glass-transition temperature was used.

Using the proposed approach, the shelf life (crystallization onset) of an ASD can now be predicted for any API load, temperature and relative humidity. In addition to the shelf life, the viscosity of the ASD can now also be estimated by applying the modeling approach in reverse, i.e. using existing crystallization-kinetics measurements far below the glass transition. The proposed modeling approach for predicting the shelf life is generally applicable to a broad range of ASDs.

This approach resulted in an $R^2 > 94\%$ accuracy for the investigated systems GRI/PVPVA and GRI/Soluplus. Besides being very accurate it requires remarkably little information. Viscosity parameters for the commonly considered ASD polymers are often already known or only need to be determined once per polymer. Thus, at the beginning of an ASD development, as little as one single DSC measurement for simultaneously determining the solubility/supersaturation and the glass-transition temperatures and one crystallization-kinetics measurement above and one below the glass transition temperature (for determining the crystallization parameters k' and B and the Arrhenius parameters, respectively) is sufficient to generate an early-stage prediction of the shelf life of a potential ASD. Within a few days to weeks, a reasonable shelf-life estimation for early ASD development is available, which can be refined with additional data as development continues.

Author contributions

The manuscript was written through contributions of all authors. All authors have approved the final version of the manuscript.

Funding sources

This research did not receive any specific grant from funding agencies in the public, commercial or not-for-profit sectors. This work was financed by the Drug Delivery Innovation Center (DDIC), INVITE GmbH, Leverkusen (Germany).

CRediT authorship contribution statement

Friederike Wolbert: Conceptualization, Formal analysis, Investigation, Methodology, Writing – original draft, Writing – review & editing. **Christian Luebbert:** Conceptualization, Methodology, Writing – review & editing. **Gabriele Sadowski:** Resources, Supervision, Writing – review & editing.

Declaration of Competing Interest

The authors declare that they have no known competing financial interests or personal relationships that could have appeared to influence the work reported in this paper.

Data availability

Data will be made available on request.

Appendix A. Supplementary data

Supplementary data to this article can be found online at https://doi.org/10.1016/j.ijpx.2023.100207.

References

Andronis, V., Zografi, G., 2000. Crystal nucleation and growth of indomethacin polymorphs from the amorphous state. J. Non-Cryst. Solids 271 (3), 236–248. https://doi.org/10.1016/S0022-3093(00)00107-1.

Avrami, M., 1939. Kinetics of phase change. I general theory. J. Chem. Phys. 7 (12), 1103–1112. https://doi.org/10.1063/1.1750380.

Avrami, M., 1940. Kinetics of phase change. II Transformation-time relations for random distribution of nuclei. J. Chem. Phys. 8 (2), 212–224. https://doi.org/10.1063/1.1750631.

Bochmann, E.S., Neumann, D., Gryczke, A., Wagner, K.G., 2016. Micro-scale prediction method for API-solubility in polymeric matrices and process model for forming amorphous solid dispersion by hot-melt extrusion. Eur. J. Pharm. Biopharm. 107, 40–48. https://doi.org/10.1016/j.ejpb.2016.06.015.

Calvin, D.W., Reed, T.M., 1971. Mixture rules for the Mie (n, 6) intermolecular pair potential and the Dymond–Alder pair potential. J. Chem. Phys. 54 (9), 3733–3738. https://doi.org/10.1063/1.1675422.

Cameretti, L.F., Sadowski, G., 2008. Modeling of aqueous amino acid and polypeptide solutions with PC-SAFT. Chem. Eng. Process. 47 (6), 1018–1025. https://doi.org/10.1016/j.cep.2007.02.034.

Christian, J.W., 2003. The theory of transformations in metals and alloys. Mater. Today 6 (3), 53. https://doi.org/10.1016/S1369-7021(03)00335-3.

Ferry, J.D., 1980. Viscoelastic Properties of Polymers. John Wiley & Sons.

Flügel, K., Hennig, R., Thommes, M., 2020. Impact of structural relaxation on mechanical properties of amorphous polymers. Eur. J. Pharm. Biopharm.: Off. J. Arbeitsgemeinschaft Pharm. Verfahrenstechnik e.V 2020 (154), 214–221. https://doi.org/10.1016/j.ejpb.2020.07.016. Published Online: Jul. 20.

Gordon, M., Taylor, J.S., 1952. Ideal copolymers and the second-order transitions of synthetic rubbers. i. Non-crystalline copolymers. J. Appl. Chem. 2 (9), 493–500. https://doi.org/10.1002/jctb.5010020901.

Greco, S., Authelin, J.-R., Leveder, C., Segalini, A., 2012. A practical method to predict physical stability of amorphous solid dispersions. Pharm. Res. 29 (10), 2792–2805. https://doi.org/10.1007/s11095-012-0717-5.

Gross, J., Sadowski, G., 2001. Perturbed-chain SAFT: an equation of state based on a perturbation theory for chain molecules. Ind. Eng. Chem. Res. 40 (4), 1244–1260. https://doi.org/10.1021/ie0003887.

Gutzow, Ivan, 1977. The mechanism of crystal growth in glass forming systems. J. Cryst. Growth 15–23.

Hallbrucker, A., Mayer, E., Johari, G.P., 1989. The heat capacity and glass transition of hyperquenched glassy water. Philos. Mag. B 60 (2), 179–187. https://doi.org/10.1080/13642818908211189.

Jackson, K.A., 1969. On the theory of crystal growth: the fundamental rate equation. J. Cryst. Growth 5 (1), 13–18. https://doi.org/10.1016/0022-0248(69)90071-2.

Jelinska, N., Kalnins, M., Tupureina, V., Dzene, A., 2010. Poly (vinyl alcohol)/poly (vinyl acetate) blend films. Sci. J. Riga Tech. Univ. 21 (1), 55–61.

Kalikmanov, V.I., 2013. Classical nucleation theory. In: Nucleation Theory. Springer, Netherlands, pp. 17–41. https://doi.org/10.1007/978-90-481-3643-8_3.

Lehmkemper, K., Kyeremateng, S.O., Heinzerling, O., Degenhardt, M., Sadowski, G., 2017. Long-term physical stability of PVP- and PVPVA-amorphous solid dispersions. Mol. Pharm. 14 (1), 157–171. https://doi.org/10.1021/acs.molpharmaceut.6b00763.

Liu, B., Theil, F., Lehmkemper, K., Gessner, D., Li, Y., van Lishaut, H., 2021. Crystallization risk assessment of amorphous solid dispersions by physical shelf-life modeling: a practical approach. Mol. Pharm. https://doi.org/10.1021/acs.molpharmaceut.1c00270. Published Online: May. 25, 2021.

Luebbert, C., Sadowski, G., 2017. Moisture-induced phase separation and recrystallization in amorphous solid dispersions. Int. J. Pharmaceut. 532 (1), 635–646. https://doi.org/10.1016/j.ijpharm.2017.08.121.

Luebbert, C., Wessner, M., Sadowski, G., 2018. Mutual impact of phase separation/crystallization and water sorption in amorphous solid dispersions. Mol. Pharm. 15 (2), 669–678. https://doi.org/10.1021/acs.molpharmaceut.7b01076.

Marsac, P.J., Konno, H., Rumondor, A.C.F., Taylor, L.S., 2008. Recrystallization of nifedipine and felodipine from amorphous molecular level solid dispersions containing poly(vinylpyrrolidone) and sorbed water. Pharm. Res. 25 (3), 647–656. https://doi.org/10.1007/s11095-007-9420-3.

Mistry, P., Suryanarayanan, R., 2016. Strength of drug–polymer interactions: implications for crystallization in dispersions. Cryst. Growth Des. 16 (9), 5141–5149. https://doi.org/10.1021/acs.cgd.6b00714.

Mueller, F., Heuwers, B., Katzenberg, F., Tiller, J.C., Sadowski, G., 2010. Tensile creep measurements of glassy VOC-loaded polymers. Macromol. (Wash. DC, U. S.) 43 (21), 8997–9003. https://doi.org/10.1021/ma101782d.

Mullin, J.W., 2001. Crystallization, 4. Aufl.; Elsevier professional.

Newman, A. (Ed.), 2015. Pharmaceutical Amorphous Solid Dispersions. Wiley.

Nucleation Theory, 2013. Springer, Netherlands.

Ojo, A.T., Lee, P.I., 2021. A mechanistic model for predicting the physical stability of amorphous solid dispersions. J. Pharm. Sci. 110 (4), 1495–1512. https://doi.org/10.1016/j.xphs.2020.08.006. Published Online: Aug. 18, 2020.

Osswald, T., Rudolph, N., 2014. Polymer Rheology: Fundamentals and Applications. Hanser eLibrary; Hanser.

Paus, R., Ji, Y., Vahle, L., Sadowski, G., 2015. Predicting the solubility advantage of amorphous pharmaceuticals:a novel thermodynamic approach. Mol. Pharm. 12 (8), 2823–2833. https://doi.org/10.1021/mp500824d.

Prudic, A., Kleetz, T., Korf, M., Ji, Y., Sadowski, G., 2014. Influence of copolymer composition on the phase behavior of solid dispersions. Mol. Pharm. 11 (11), 4189–4198. https://doi.org/10.1021/mp500412d.

Rask, M.B., Knopp, M.M., Olesen, N.E., Holm, R., Rades, T., 2018. Comparison of two DSC-based methods to predict drug-polymer solubility. Int. J. Pharmaceut. 540 (1–2), 98–105. https://doi.org/10.1016/j.ijpharm.2018.02.002.

Simha, R., Boyer, R.F., 1962. On a general relation involving the glass temperature and coefficients of expansion of polymers. J. Chem. Phys. 37 (5), 1003–1007.

Six, K., Verreck, G., Peeters, J., Brewster, M., van den Mooter, G., 2004. Increased physical stability and improved dissolution properties of itraconazole, a class II drug, by solid dispersions that combine fast- and slow-dissolving polymers. J. Pharm. Sci. 93 (1), 124–131. https://doi.org/10.1002/jps.10522.

Todinov, M., 2000. On some limitations of the Johnson–Mehl–Avrami–Kolmogorov equation. Acta Mater. 48 (17), 4217–4224. https://doi.org/10.1016/S1359-6454(00)00280-9.

Tumakaka, F., Gross, J., Sadowski, G., 2002. Modeling of polymer phase equilibria using Perturbed-Chain SAFT. Fluid Phase Equilib. 194-197, 541–551. https://doi.org/10.1016/S0378-3812(01)00785-3.

Tung, H.-H., Paul, E.L., Midler, M., McCauley, J.A., 2009. Crystallization of Organic Compounds: An Industrial Perspective. John Wiley & Sons.

Williams, M.L., Ferry, J.D., 1954. Dynamic mechanical properties of polyvinyl acetate. J. Colloid Sci. 9 (5), 479–492. https://doi.org/10.1016/0095-8522(54)90035-5.

Williams, M.L., Landel, R.F., Ferry, J.D., 1955. The temperature dependence of relaxation mechanisms in amorphous polymers and other glass-forming liquids. J. Am. Chem. Soc. 77 (14), 3701–3707.

Wolbach, J.P., Sandler, S.I., 1998. Using molecular orbital calculations to describe the phase behavior of cross-associating mixtures. Ind. Eng. Chem. Res. 37 (8), 2917–2928. https://doi.org/10.1021/ie9707811.

Wolbert, F., Stecker, J., Luebbert, C., Sadowski, G., 2020. Viscosity of ASDs at humid conditions. Eur. J. Pharm. Biopharm. 154, 387–396. https://doi.org/10.1016/j.ejpb.2020.07.024.

Wolbert, F., Nikoleit, K., Steinbrink, M., Luebbert, C., Sadowski, G., 2022a. The shelf life of ASDs: 1. Measuring the crystallization kinetics at humid conditions. Mol. Pharm. 19 (7), 2483–2494. https://doi.org/10.1021/acs.molpharmaceut.2c00188. Published Online: Jun. 21, 2022.

Wolbert, F., Fahrig, I.-K., Gottschalk, T., Luebbert, C., Thommes, M., Sadowski, G., 2022b. Factors influencing the crystallization-onset time of metastable ASDs. Pharmaceutics 14 (2), 269. https://doi.org/10.3390/pharmaceutics14020269.

Yang, J., Grey, K., Doney, J., 2010. An improved kinetics approach to describe the physical stability of amorphous solid dispersions. Int. J. Pharmaceut. 384 (1–2), 24–31. https://doi.org/10.1016/j.ijpharm.2009.09.035.

Zhou, D., Zhang, G.G.Z., Law, D., Grant, D.J.W., Schmitt, E.A., 2008. Thermodynamics, molecular mobility and crystallization kinetics of amorphous griseofulvin. Mol. Pharm. 5 (6), 927–936. https://doi.org/10.1021/mp800169g.